

1 Electronic Supplemental Information - Valentin et al. "3D Printed Self-Adhesive PEGDA-PAA Hydrogels as Modular Components for Soft Actuators and Microfluidics"

Table of Contents

| Item | Section | Details | Page |
|------------|---|--|------|
| Figure S1 | PEGDA-PAA Formulation Optimization | Experimental & Decision Flowchart | 1 |
| Figure S2 | PEGDA-PAA Formulation Optimization | Precursor Soln. Formulations Table | 2 |
| Figure S3 | Rheology of PEGDA-PAA Formulations | | 3 |
| Figure S4 | Windowpane Analysis | | 4 |
| Figure S5 | Degree of Swelling Analysis | Actuation | 4 |
| Figure S6 | Degree of Swelling Analysis | Healing | 4 |
| Table S1 | XPS Analysis | PEGDA Peaks Table | 5 |
| Table S2 | XPS Analysis | PEGDA-PAA Peaks Table | 5 |
| Figure S7 | XPS Analysis | PEGDA vs PEGDA-PAA | 5 |
| Figure S8 | XPS Analysis | PEGDA-PAA (Detailed) | 6 |
| Figure S9 | Fourier-Transform Infrared Spectroscopy | | 7 |
| Figure S10 | Volumetric Swelling Analysis | | 7 |
| Figure S11 | Scanning Electron Microscopy | | 8 |
| Figure S12 | Cantilever & Gripper Drawings | | 8 |
| Figure S13 | Gripper Actuation & Relaxation | | 9 |
| Figure S14 | Self-Adhesion Rheology | | 10 |
| Figure S15 | Hydrogel Stability in DI Water & 1X PBS | | 11 |
| Figure S16 | Long-Term Self-Adhesion Stability | | 11 |
| Figure S17 | Effect of Molecular Weight on Self-Adhesion | | 12 |
| Figure S18 | LEGO Block Drawings | Straight & Stacked | 13 |
| Figure S19 | Pattern Fidelity | | 14 |
| Figure S20 | LEGO Block Drawings | Linked | 15 |
| Figure S21 | LEGO Block Drawings | Serpentine & T-Junction | 16 |
| Figure S22 | COMSOL Modeling of Chaotic Advection | Comparison of Raw Data vs. COMSOL Modeling | 17 |
| Figure S23 | T-Junction Microfluidic Device | | 18 |

1.1 PEGDA-PAA Formulation Optimization

Optimization of the PEGDA-PAA hydrogels first involved finding the pH conditions necessary to achieve a homogeneous, clear hydrogel (Figure S1). Without any pH balancing or if the pH was below 4, the hydrogels were poorly UV crosslinked and only formed weak, soft hydrogels. When pH was balanced to greater than 6, the PEGDA was cleaved and prevented crosslinking. The ideal pH was determined to be between pH 4.7-5.3, which allowed for some deprotonation and possibly a change in conformation of the PAA¹, effective UV crosslinking of the PEGDA, and stiff, clear hydrogels.

Second, the ionic tunability of hydrogel stiffness was optimized. Rheological analysis of various PEGDA and PAA formulations was performed (Figure S3). This data was analyzed to determine the formulations that exhibited the largest range of ionically tunable stiffnesses (comparing initial conditions to those treated with 1 M FeCl₃ for 24 hr). Overall, the PEGDA-PAA hydrogels with low concentrations of PAA (1% and 2.5% PAA) exhibited relatively small changes in stiffness with varying ion concentration. The PEGDA-PAA hydrogels containing 5% PAA exhibited the greatest stiffness range over varying ion concentrations. Nevertheless, hydrogels

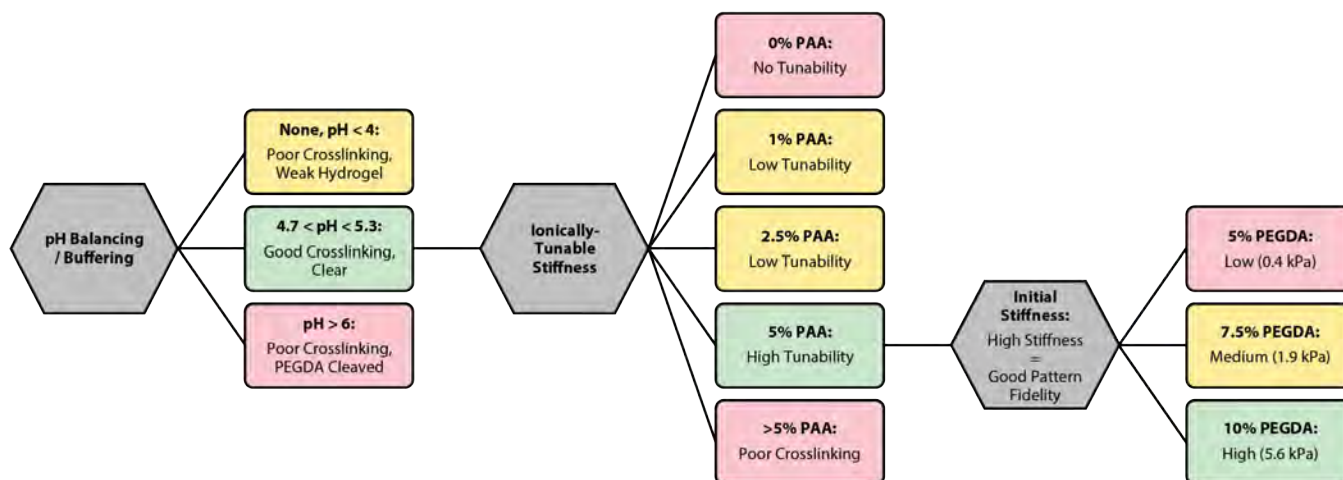


Fig. S1 Flowchart illustrating the selection criteria based on uniformity, ionic tunability, and mechanical stiffness, that led to the choice of 10% PEGDA - 5% PAA as the optimal formulation.

containing greater than 5% PAA exhibited ineffective UV crosslinking, likely due to interference of PAA in the PEGDA crosslinking. Finally, hydrogels consisting of only PEGDA did not exhibit appreciable stiffness change at varying ion concentration, since they could not be ionically crosslinked.

Finally, the mechanical stiffness after crosslinking was optimized. It was noted that pattern fidelity improved with stiffness as the hydrogel was able to better support itself in 3D. Comparing the initial PEGDA-PAA hydrogels containing 5% PAA, the 5% PEGDA hydrogels were very soft (0.4 kPa) and did not exhibit good pattern fidelity (**Figure S3**). Hydrogel stiffness improved significantly with 7.5% PEGDA (1.9 kPa), and improved even more significantly with 10% PEGDA (5.6 kPa). The 10% PEGDA formulations also exhibited the best pattern fidelity. This yielded the final selection of 10% PEGDA - 5% PAA as the optimal formulation.

| | | Volumes (μL) | | | |
|-----------|------------|---------------------------|------|------|------|
| | | [PEGDA] (%) | | | |
| [PAA] (%) | | 0 | 5 | 7.5 | 10 |
| 0 | PEGDA | 0 | 500 | 750 | 1000 |
| | 10% I-2959 | 0 | 500 | 750 | 1000 |
| | PAA | 0 | 0 | 0 | 0 |
| | 1 N NaOH | 0 | 0 | 0 | 0 |
| | DI Water | 10000 | 9000 | 8500 | 8000 |
| 1 | PEGDA | 0 | 500 | 750 | 1000 |
| | 10% I-2959 | 0 | 500 | 750 | 1000 |
| | PAA | 400 | 400 | 400 | 400 |
| | 1 N NaOH | 200 | 200 | 200 | 200 |
| | DI Water | 9400 | 8400 | 7900 | 7400 |
| 2.5 | PEGDA | 0 | 500 | 750 | 1000 |
| | 10% I-2959 | 0 | 500 | 750 | 1000 |
| | PAA | 1000 | 1000 | 1000 | 1000 |
| | 1 N NaOH | 500 | 500 | 500 | 500 |
| | DI Water | 8500 | 7500 | 7000 | 6500 |
| 5 | PEGDA | 0 | 500 | 750 | 1000 |
| | 10% I-2959 | 0 | 500 | 750 | 1000 |
| | PAA | 2000 | 2000 | 2000 | 2000 |
| | 1 N NaOH | 1333 | 1333 | 1333 | 1333 |
| | DI Water | 6667 | 5667 | 5167 | 4667 |
| 10 | PEGDA | 0 | 500 | 750 | 1000 |
| | 10% I-2959 | 0 | 500 | 750 | 1000 |
| | PAA | 4000 | 4000 | 4000 | 4000 |
| | 1 N NaOH | 2667 | 2667 | 2667 | 2667 |
| | DI Water | 3333 | 2333 | 1833 | 1333 |

Fig. S2 Volumes (μL) of PEGDA, 10% I-2959, 25% PAA, 1N NaOH and DI water stock solutions to prepare 10mL (final volume) of precursor solution.

1.2 Rheology of PEGDA-PAA Formulations

Rheological analysis was performed on various formulations of PEGDA-PAA precursor solutions ranging from 5-10% PEGDA and 0-5% PAA (Figure S3). Preliminary experiments into formulations containing >5% PAA had significant difficulty crosslinking, likely due to the PAA sterically interfering with PEGDA crosslinking. A general trend of increasing stiffness correlates with PEGDA and PAA concentration. Immersion in 1 M FeCl₃ for 24 hours yielded a large increase in stiffness for all hydrogel formulations with the exception of the 10% PEGDA only formulation. Subsequent immersion in 100 mM EDTA for 24 hours resulted in a large decrease in stiffness for all hydrogel formulations. Overall, the formulations containing 5% PAA saw the largest increase in stiffness, and the largest decrease in stiffness after immersion in 1 M FeCl₃ and 100 mM EDTA, respectively.

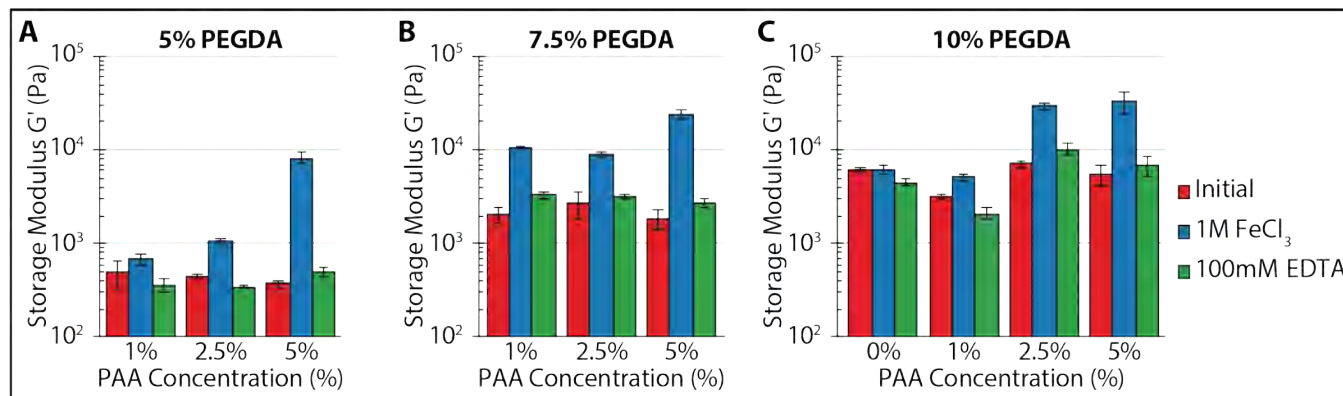


Fig. S3 Rheological characterization of PEGDA-PAA precursor solutions containing (A) 5% PEGDA, (B) 7.5% PEGDA, and (C) 10% PEGDA. Error bars = standard deviation.

1.3 Windowpane Analysis

The critical exposure (E_C) was determined empirically using a windowpane test². Known E_C and penetration depth (D_P) values were used as a starting point, and the laser scanning speed was changed to directly change the maximum exposure (E_{max}):

$$E_{max} = \frac{P_L \sqrt{2/\pi}}{W_0 V_S} \quad (1)$$

Where P_L is the laser power, W_0 is the beam width, and V_S is the laser scanning speed. The laser was scanned over the surface of a bath of hydrogel precursor solution for a 1-layer windowpane part. This crosslinked part was then lifted out of the bath using wafer tweezers. The cure depth (C_D) was determined using a contact angle goniometer and was plotted against E_{max} on a semilog plot. The x-intercept is the E_C value (Figure 1.3). The D_P value was selected from previously published values for 10% PEGDA hydrogels³.

$$C_D = D_P \ln\left(\frac{E_{max}}{E_C}\right) \quad (2)$$

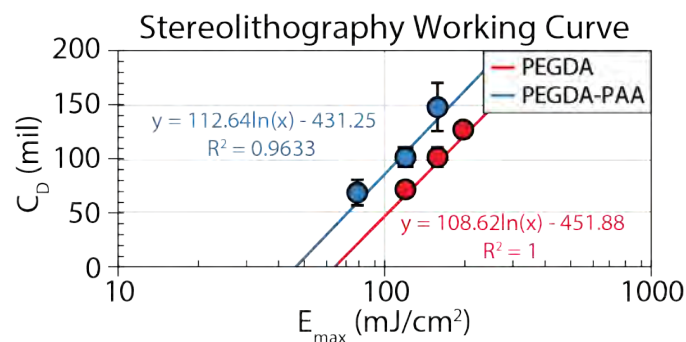


Fig. S4 Working curve for PEGDA and PEGDA-PAA precursor solutions. Error bars = standard deviation.

1.4 Degree of Swelling Analysis

Degree of swelling (DOS) was calculated for PEGDA and PEGDA-PAA hydrogels in conditions used for both hydrogel actuation (Figure S5) and self-adhesion (Figure S6).

$$DOS = 100 \left(\frac{m_{wet} - m_{dry}}{m_{dry}} \right) \quad (3)$$

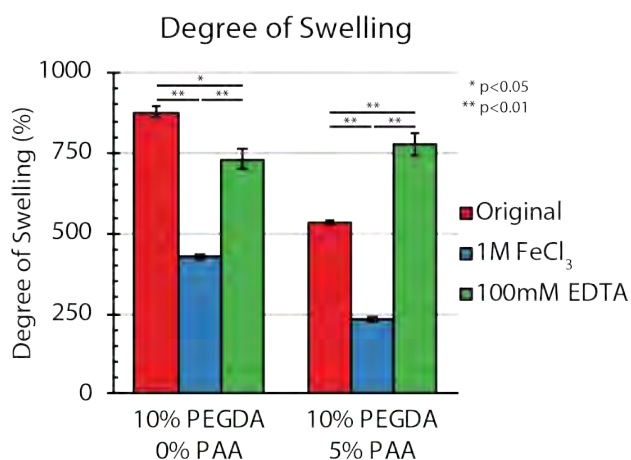


Fig. S5 Degree of Swelling for hydrogels and treatment conditions used for hydrogel actuation. Error bars = standard deviation. * $p < 0.05$ ** $p < 0.01$ (Student's t-test).

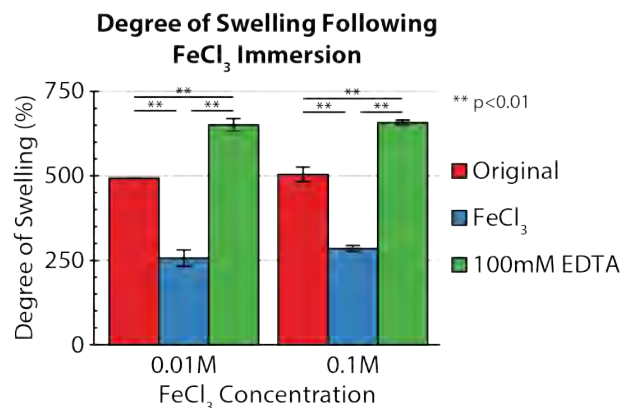


Fig. S6 Degree of Swelling for PEGDA-PAA hydrogels after immersion in 0.01, and 0.1 M FeCl_3 in 1X PBS. Error bars = standard deviation. * $p < 0.05$ ** $p < 0.01$ (Student's t-test).

Table S2 Elements and binding energies (BE) for peaks detected during XPS of PEGDA-PAA hydrogels.

| Sample/Element | Peak BE (eV) | Ref. |
|----------------------------|--------------|-------|
| Initial | | |
| C1s | 284.65 | 4 |
| | 285.92 | 4 |
| | 288.53 | 4 |
| O1s | 532.38 | 4 |
| 1M FeCl₃ | | |
| C1s | 284.58 | 4 |
| | 285.93 | 4 |
| | 288.92 | 4 |
| O1s | 532.27 | 5 |
| Fe2p _{3/2} | 711.03 | 5-7 |
| | 715.36 | 5,8 |
| Fe2p _{1/2} | 724.28 | 5-7 |
| | 728.94 | 5,8 |
| Cl2p | 198.96 | 7 |
| 100mM EDTA | | |
| C1s | 284.29 | 4 |
| | 285.83 | 4 |
| | 288.17 | 4 |
| O1s | 530.19 | 5,7,9 |
| | 532.14 | 4 |
| Cl2p | 198.28 | 7 |
| Na1s | 1070.98 | 9 |

Table S1 Elements and binding energies (BE) for peaks detected during XPS of PEGDA hydrogels.

| Sample/Element | Peak BE (eV) | Ref. |
|----------------------------|--------------|------|
| 1M FeCl₃ | | |
| C1s | 284.8 | 4 |
| | 286.44 | 4 |
| | 286.86 | 4 |
| O1s | 532.91 | 4,5 |
| Fe2p _{3/2} | 711.29 | 5-7 |
| | 716.07 | 5,8 |
| Fe2p _{1/2} | 724.09 | 5-7 |
| Cl2p | 729.4 | 5,8 |
| | 199.4 | 7 |

1.5 XPS Analysis

X-Ray Photoelectron Spectroscopy (XPS) was performed on PEGDA and PEGDA-PAA in their initial formulations, after being immersed in 1 M FeCl₃ for 24 hours, and subsequently immersed in 100 mM EDTA for 24 hours. A detailed table of peaks, binding energies, and peak assignments can be found in **Tables S1-S2**.

XPS analysis was performed on PEGDA hydrogels to compare the 1 M FeCl₃ condition against that of the PEGDA-PAA hydrogels (**Figure S7**). A doublet structure is observed for both conditions due to the spin-orbit splitting (Fe2p_{1/2} and Fe2p_{3/2}), with binding

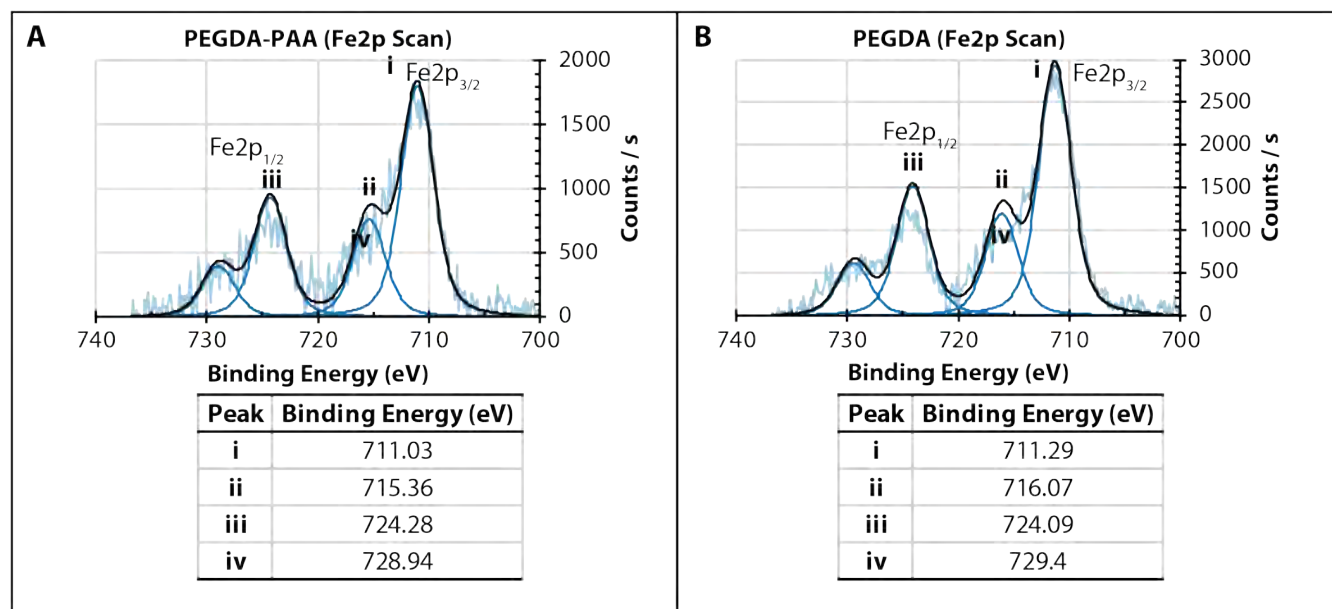


Fig. S7 XPS Iron spectrum for PEGDA-PAA (A) and PEGDA (B) hydrogels, showing two doublets.

energies of 711.03 eV and 715.36 eV for PEGDA-PAA and 711.29 eV and 716.07 eV for PEGDA. Additionally, two satellite peaks are observed for both conditions which is indicative for an oxidation state of Fe(III).⁷ XPS analysis of the original PEGDA-PAA hydrogels (**Figure S8**) showed three carbon peaks, a single oxygen peak, and no iron peaks. The three carbon peaks are associated with C-C, C-H, C-OH, C-O-C and O-C=O. The oxygen peak is associated with aliphatic O-(C=O*)-C bonds (* indicates element of interest). As expected no iron peaks were seen. Following immersion in 1 M FeCl₃ the three carbon peaks remain, along with the oxygen peak. Iron doublets also appeared, associated with the oxidation state of Fe(III). Following immersion in 100 mM EDTA in 1X PBS, the three carbon peaks remain. Two oxygen peaks were seen that are associated with aliphatic O-(C=O*)-C bonds. Two small sodium and chlorine peaks were also seen (not shown), and are likely due to the 1X PBS.

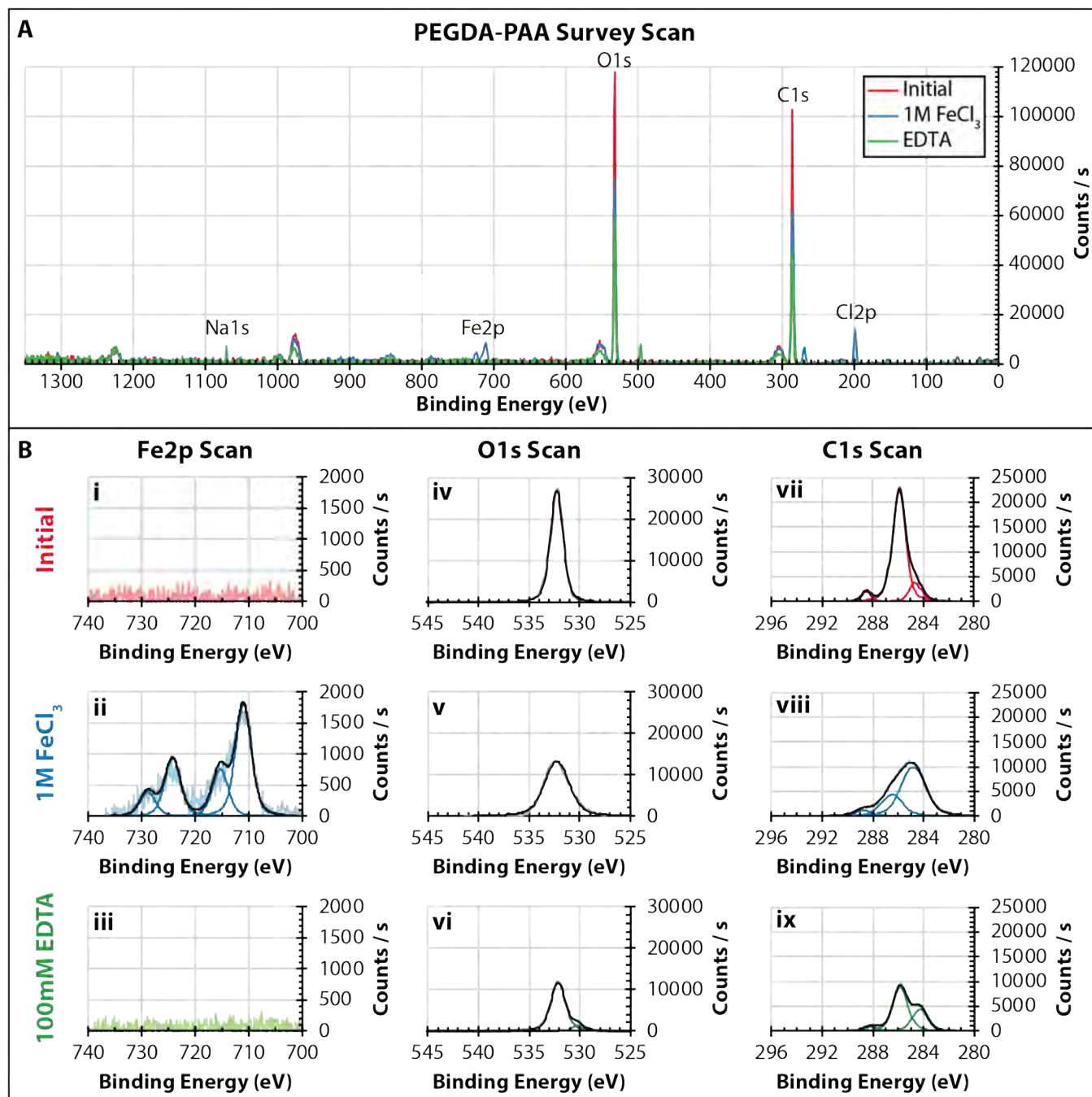


Fig. S8 XPS spectra for Carbon, Oxygen, and Iron for (i-iii) Original, (iv-vi) FeCl₃-cured, and (vii-ix) 100 mM EDTA PEGDA-PAA hydrogels.

1.6 Fourier-Transform Infrared Spectroscopy

FTIR analysis was performed on the PEGDA-PAA and PEGDA hydrogels, as well as water, 5% PAA, and 5% PAA with 1M FeCl₃ (Figure S9). PEGDA-PAA and PEGDA hydrogels were analyzed as-printed (original), after immersion in 1 M FeCl₃, and after immersion in 100 mM EDTA (following 1 M FeCl₃) for 24 hours. Distinct peaks associated with carboxyl groups appeared with the addition of PAA to the 10% PEGDA hydrogels. Some of these peaks might have been masked by a water peak but they become more visible after immersion in 1 M FeCl₃ for 24 hours due to shrinkage of the hydrogels and decreased degree of swelling.

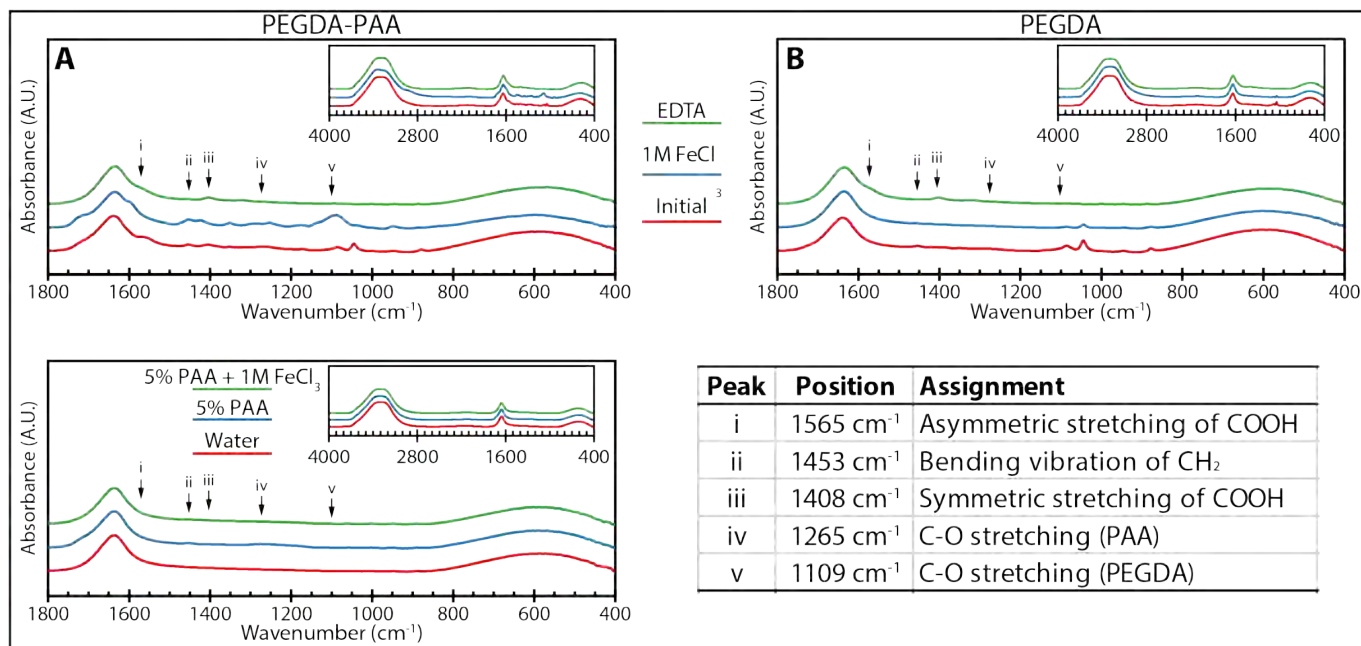


Fig. S9 FTIR spectra for (A) PEGDA-PAA, (B) PEGDA, and (C) PAA, PAA + FeCl₃, and water controls. Peaks were identified at (i) 1565 cm⁻¹¹⁰, (ii) 1453 cm⁻¹^{10,11}, (iii) 1408 cm⁻¹¹⁰, (iv) 1265 cm⁻¹¹², (v) 1109 cm⁻¹¹³.

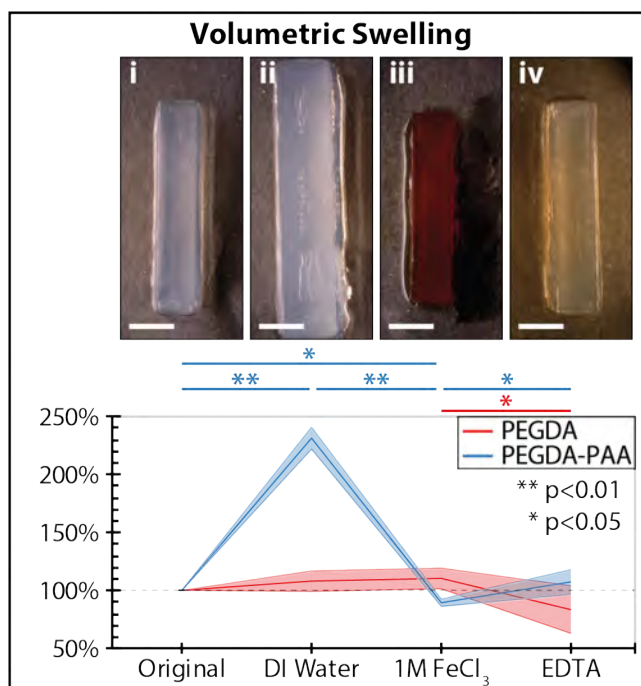


Fig. S10 Plot of volumetric swelling of PEGDA and PEGDA-PAA Stereolithographically printed (i) original hydrogels, and after immersion in (ii) water, (iii) 1 M FeCl₃, and (iv) EDTA for 24 hrs. Scale bars = 5 mm. Shaded error bars = standard deviation * p<0.05, ** p<0.01 (Student's t-test).

1.7 Volumetric Swelling Analysis

Differential swelling and contraction of PEGDA and PEGDA-PAA hydrogels (**Figure S10**) was harnessed to create hydrogel actuation using cantilever beams. This volumetric swelling of Stereolithographically printed-printing 4x4x20 mm rectangles was quantified by imaging them from above and from the side to calculate an approximate volume. Immersion in DI water caused a significant 2.3-fold increase in hydrogel swelling, followed by a significant 2.6-fold decrease in volume after immersion in 1 M FeCl₃. Immersion in EDTA then caused a significant 1.2-fold increase in volume.

1.8 Scanning Electron Microscopy

Preparation of PEGDA-PAA hydrogels for SEM involved freezing overnight at -80°C. PEGDA-PAA were then lyophilized overnight using a LABCONCO FreeZone 6 Liter Freeze Dry System and sputter-coated with a 10 nm layer of 80:20 Pt:Pd (19.56 g/m³) at 40 mA using a Quorum EMS 150T S Metal Sputter Coater. Microscopy was performed using a Zeiss Supra55VP Field Emission Scanning Electron Microscope (FESEM), using the InLens detector, and an acceleration voltage of 5 kV. Images were acquired using 30 second frame averaging. The sputter coater and SEM were located at Harvard University's Center for Nanoscale Systems Electron Microscopy Facility. SEM of a Stereolithographically printed PEGDA-PAA hydrogel showed a porous internal structure. The individual Stereolithographically printed layers were also easily visible in a PEGDA-PAA hydrogel after immersion in 1 M FeCl₃ (**Figure S11**).

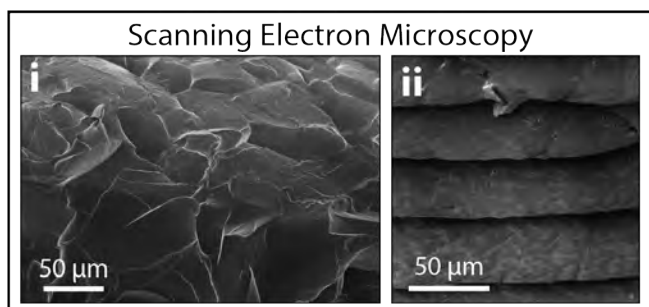


Fig. S11 SEM images of the (i) interior of an initially-printed PEGDA-PAA hydrogel and (ii) Stereolithographically printed layers of a PEGDA-PAA 1 M FeCl₃-cured hydrogel.

1.9 Cantilever & Gripper Drawings

Bending and Twisting cantilevers were fabricated using the following dimensions (**Figure S12**). PEGDA and PEGDA-PAA layers were assembled as shown in **Figure 3**, with PEGDA being printed first, followed by PEGDA-PAA. All units are in millimeters.

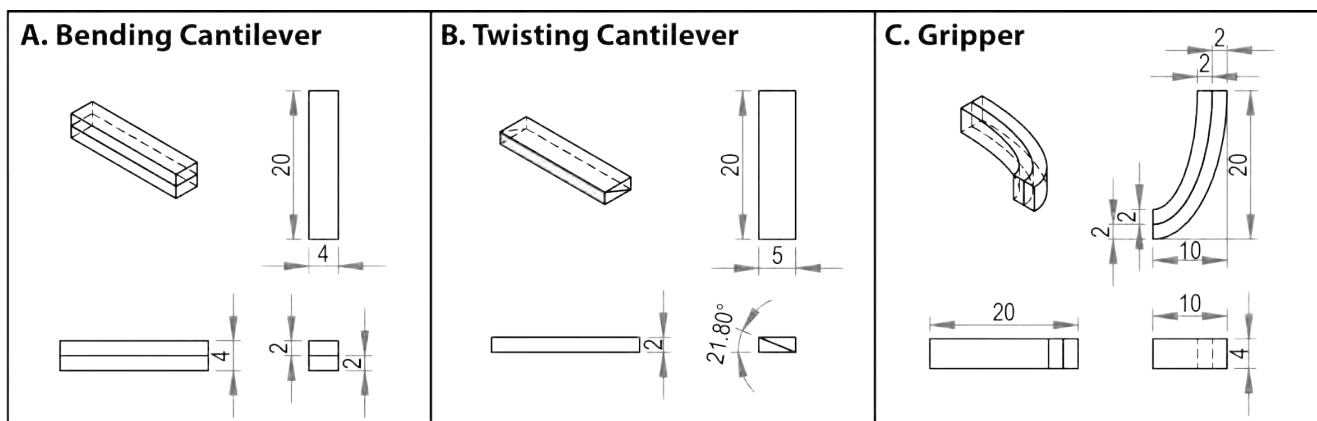


Fig. S12 Dimensioned drawings for (A) bending and (B) twisting cantilevers, and (C) gripper. All units are in mm. Dashed lines indicate hidden lines.

1.10 Gripper Actuation & Relaxation

To quantify gripper actuation, printed grippers were immersed in 1 M FeCl_3 for 60 minutes and imaged every 5 minutes. After 60 minutes, the FeCl_3 was removed and the grippers were immersed in 100 mM EDTA for 20 hours and imaged every 30 minutes. The radius of curvature was calculated similar to the cantilevers.

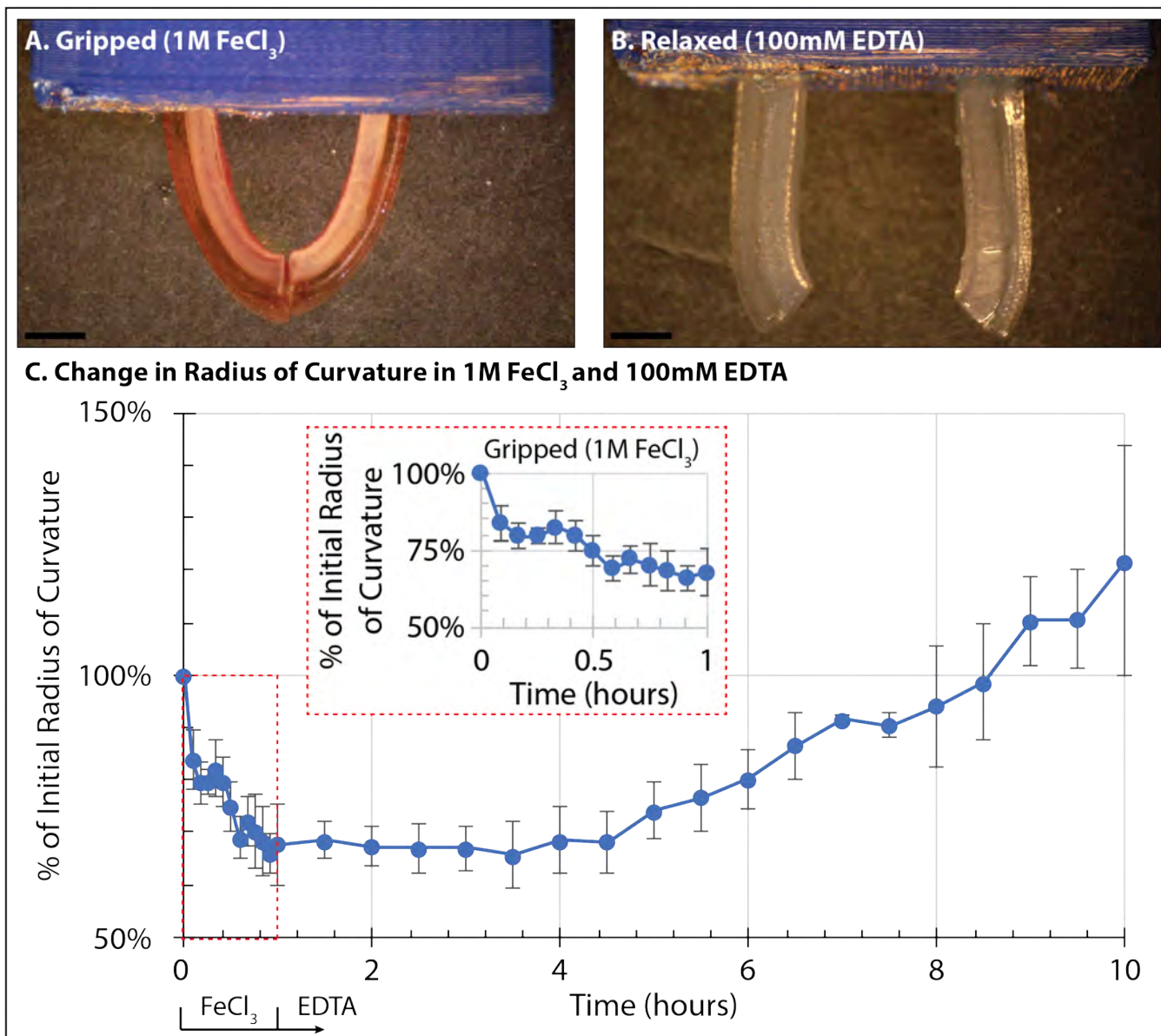


Fig. S13 (A) PEGDA-PAA grippers were actuated in 1 M FeCl_3 for 35 minutes, and (B) allowed to relax after being immersed in 100 mM EDTA for 24 hours (EDTA was changed after 12 hours). Scale bars = 5 mm. (C) Quantification of the change in mean radius of curvature for grippers immersed in 1M FeCl_3 for 60 minutes, and then immersed in 100 mM EDTA for 9 hours (EDTA was changed after 12 hours). The decrease in radius of curvature levels out at $t \approx 30$ minutes in 1 M FeCl_3 (red inset box). After immersion in 100 mM EDTA at $t = 1$ hour, the grippers return to their original radius of curvature by $t \approx 8$ hours. Error bars = standard deviation.

1.11 Self-Adhesion Rheology

Self-adhesion was quantified over time using shear rheology (**Figure S14**). 8 mm diameter and 1.5 mm tall PEGDA-PAA discs were stacked on top of each other and placed in the rheometer. The cylinders were allowed to equilibrate on the rheometer for 2 min and then immersed in 0.01 and 0.1 M FeCl₃ for 20 min. The storage modulus of these cylinders was observed over time using a time sweep (**Figure S14A**). The storage modulus increased significantly over 1 min. and then plateaued, remaining relatively consistent for the remainder of the time sweep. The 0.1 M FeCl₃ reached a significantly higher storage modulus than 0.01 M FeCl₃ after 20 min. After 24 hours

As a control, 8 mm diameter and 3 mm tall cylinders were prepared out of PEGDA-PAA (**Figure S14B**). The cylinders were allowed to equilibrate on the rheometer for 2 min and then immersed in 0.01 and 0.1 M FeCl₃ for 20 min. The storage modulus of these cylinders was observed over time using a time sweep. Similar to the stacked discs, the storage modulus increased dramatically over 1 min. but then plateaued for the 0.1 M FeCl₃ condition. For the 0.01 M FeCl₃ condition, a rapid increase was seen after 1 min., but a gradual increase in storage modulus continued over 20 min., likely due to Fe³⁺ diffusing into the center of the cylinder.

Stacked discs were first compared against the solid cylinders in the absence of FeCl₃ and showed a significantly lower storage modulus compared to the solid cylinder (**Figure S14C**). After 20 min. there was not a statistically significant difference between the stacked discs immersed in 0.01 vs 0.1 M FeCl₃. However, after 24 hrs. the difference between the stacked discs immersed in 0.01 vs. 0.1 M FeCl₃ was statistically significant ($p < 0.01$). A similar trend was seen with the solid cylinders where there the difference between 0.01 vs 0.1 M FeCl₃ was not statistically significant, whereas after 24 hrs. the difference increased dramatically and was statistically significant ($p < 0.05$). The standard deviations of the stacked discs and solid cylinders decreased over 24 hrs., likely due to FeCl₃ diffusing through the entirety of the hydrogels and uniformly crosslinking them.

Stacked discs and solid cylinders of PEGDA were also immersed in FeCl₃ for 24 hrs (**Figure S14D**). As expected these hydrogels showed no significant increase over time. There was a significant difference between stacked discs and solid cylinders initially, but this difference was no longer significant after immersion in FeCl₃.

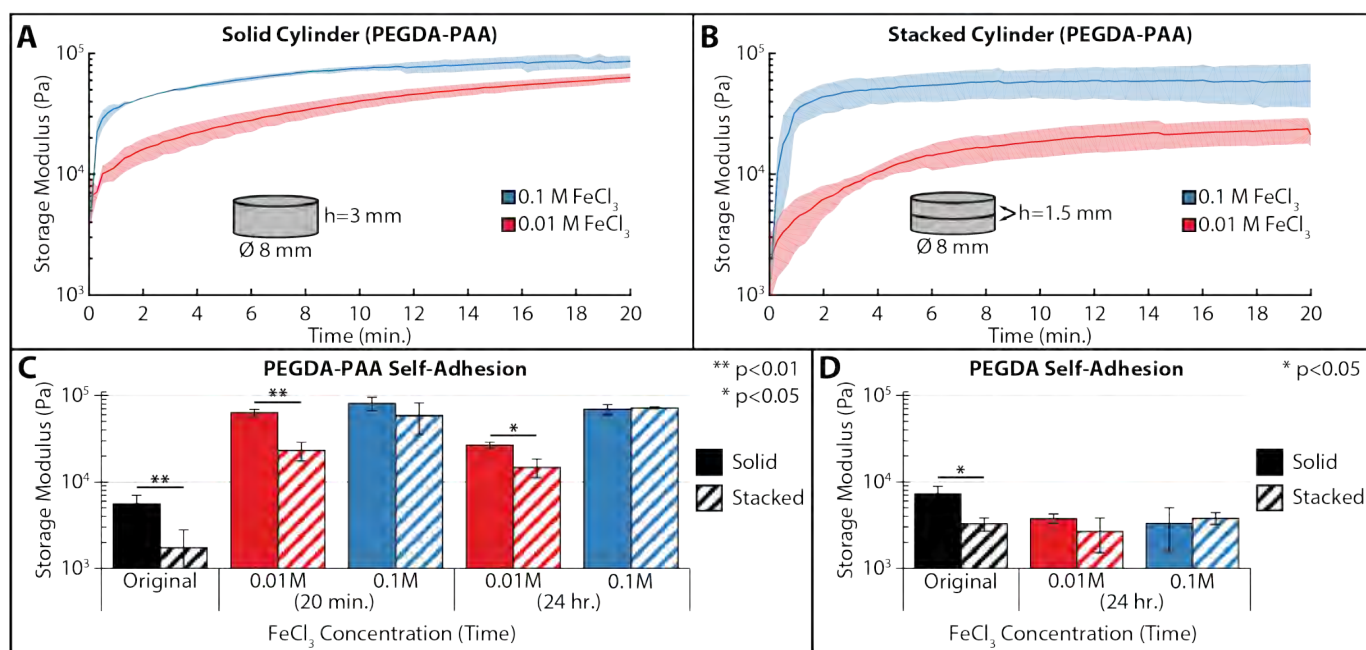


Fig. S14 20 min. rheological time sweeps in 0.01 and 0.1 M FeCl₃ of stacked PEGDA-PAA discs (**A**) and solid PEGDA-PAA cylinders (**B**). Shaded error bars = standard deviation. (**C**) Storage modulus of stacked and solid original PEGDA-PAA hydrogels, and following immersion in 0.01 and 0.1 M FeCl₃ for 20 min. and 24 hrs. (**D**) Storage modulus of stacked and solid original PEGDA hydrogels, and following immersion in 0.01 and 0.1 M FeCl₃ for 24 hrs. Error bars = standard deviation. * $p < 0.05$ ** $p < 0.01$ (Student's t-test).

1.12 Hydrogel Stability in DI Water & 1X PBS

PEGDA and PEGDA-PAA stability in DI water and 1X PBS was evaluated over 10 days, and the increase in cross-sectional area was quantified using Image-J. Over 10 days in DI water and 1X PBS, PEGDA-PAA hydrogels swelled dramatically in DI water (**Figure S15A**) and the cross-sectional area increased by 121 mm² or 250%. In 1X PBS, however, the PEGDA-PAA hydrogels swelled significantly less (**Figure S15A**) and the cross-sectional area increased by 53 mm² or 157%, a significant decrease ($p = 0.028$, student's t-test) from DI water. Over the same time period, the PEGDA hydrogels showed very little swelling (**Figure S15B**) and the cross-sectional areas after immersion in DI Water and 1X PBS were not statistically significant. This demonstrates how swelling can be controlled using FeCl₃

prepared in 1X PBS versus DI water. For this reason, self-adhesion was performed using 0.1 M FeCl₃ in 1X PBS.

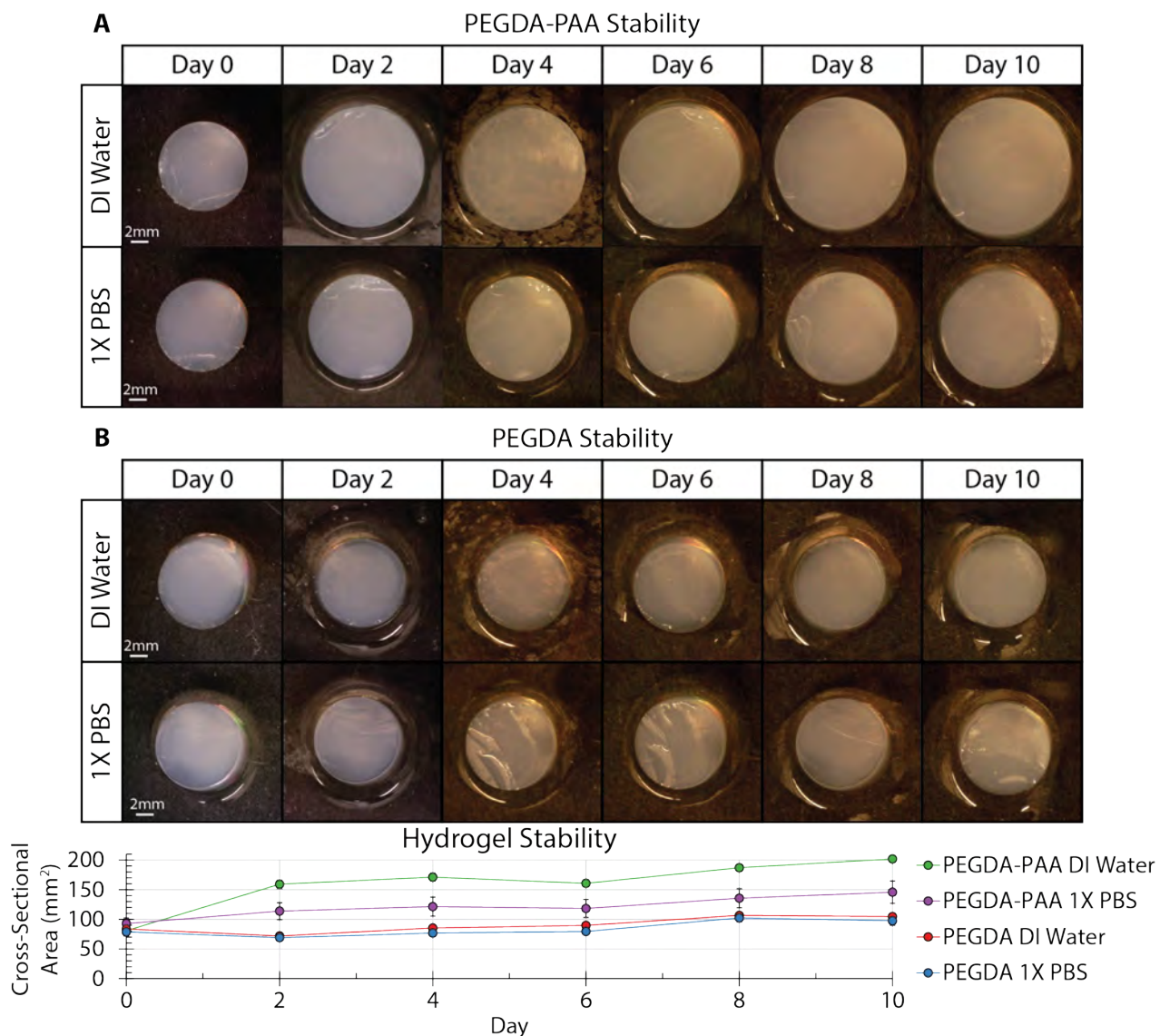


Fig. S15 Images demonstrating the stability of PEGDA-PAA (**A**) and PEGDA (**B**) hydrogels immersed in DI water and 1X PBS for 10 days. Cross-sectional area measured with Image-J. Error bars = standard deviation.

1.13 Long-Term Self-Adhesion Stability

To evaluate the stability of healed PEGDA-PAA hydrogels, rectangular blocks were adhered together in 0.1 M FeCl₃ in 1X PBS for 1 hour. The adhered blocks were subsequently stored in 1X PBS or DI water for 10 days and imaged every 2 days (**Figure S16**). Over 10 days



Fig. S16 10 day long-term stability of self-adhered PEGDA-PAA hydrogels in DI.

the adhered blocks stored in DI water showed some deformation but overall remained well adhered. Conversely, the adhered blocks stored in 1X PBS showed significant swelling and all adhesion was lost by day 10. This is likely due to chelation of the Fe^{3+} by the phosphates in PBS. For this reason, any self-adhered PEGDA-PAA hydrogels should be stored in DI water, not PBS for long-term storage. It is likely that DI water with ≈ 0.133 M NaCl would also be adequate.

1.14 Effect of Molecular Weight on Self-Adhesion

To investigate the effect of molecular weight on self-adhesion, we examined four different hydrogel compositions. All four conditions were prepared at a ratio of 10% PEGDA - 5% PAA as described in **Figure S2**. The PAA was held at a concentration of 5 (w/v%) and the PEGDA at 10 (w/v%), such that each sample had a similar number of functional groups. The precursor solutions were then crosslinked under a UV flood lamp for 20 minutes. The 8 mm diameter cylinders were then sliced into 3mm pieces and adhered together using 0.1 M FeCl_3 in 1X PBS for 60 min. Self-adhered hydrogels were then mechanically agitated and subsequently imaged (**Figure S17**).

Effect of Molecular Weight on Self-Adhesion

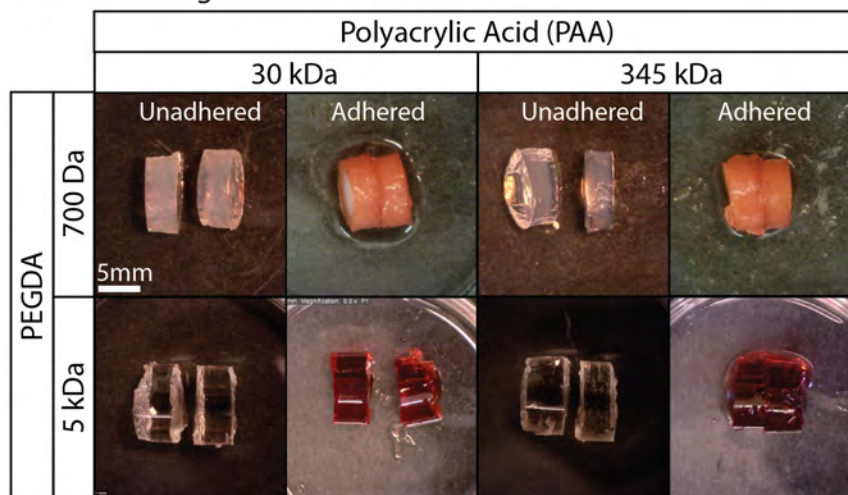


Fig. S17 Self-adhesion of hydrogels comprised of varying molecular weight 10% w/v PEGDA (700 Da, 5 kDa) and 10% PAA (30 kDa, 345 kDa)

1.15 Flexural Testing

For Instron flexural testing (**Figure 5**) the rate of crosshead motion (R), terminal displacement (D_T), and flexural modulus (E_f) are given by:

$$R = \frac{ZL^2}{6d} = 0.67 \frac{\text{mm}}{\text{min}} \quad D_T = \frac{r_T L^2}{6d} = 3.33 \text{mm} \quad E_f = \frac{L^3 m}{4bd^3} \quad (4)$$

where $Z = 0.01$ and is the rate of straining of the outer fiber, L is the span between the supports, d is the thickness of the sample, $r_T = 0.05$ and terminal strain, m is the slope of the tangent to the initial straight-line portion of the load-displacement curve, and b is the width of the beam¹⁴.

1.16 LEGO Microfluidic Fabrication

The channels for all fabricated LEGO blocks were 1 mm deep, and 2 mm wide square channels. In practice these channels ended up being round due to overcure. The inlet and outlet ports were biopsy punched with a 2 mm biopsy punch. The bulk of the LEGO blocks were fabricated to be 2 mm tall. For the male blocks, the connectors were 0.75 mm tall and 1.25 mm in diameter, with a draft angle of 10 degrees. For the female blocks, the connectors were 1 mm deep and 1.25 mm in diameter. Connectors were positioned 6.25 mm apart in x and y, with the exception being for the serpentine and overlapping channels where some connectors were omitted. For the overlapping channels, the blocks were both fabricated as 20 mm x 20 mm squares.

For perfusion, inlet and outlet ports were connected to a Harvard Apparatus Harvard Pump 11 Elite Pico Plus syringe pump using 5 mL syringes, 1/16" luer barbed fittings, Masterklear Clear 1/16" ID, 1/8" OD PVC tubing, and 1-1/2" long, 14 gauge stainless steel dispensing needles with Luer Lock connection and a 90 degree angle. Perfusion was at 0.2 mL / min at the outlet, meaning that for the T-Junction and serpentine mixer, the inlet flow rate was 0.1 mL/min. Perfusion took place under negative pressure to minimize bubbles.

1.17 LEGO Block Drawings

LEGO-style PEGDA-PAA blocks were fabricated using the following dimensions (Figure S18-S21). All male and female connectors were identical across LEGO designs. The pattern and spacing of the connectors did change as needed by the microfluidic channel requirements. All units are in millimeters.

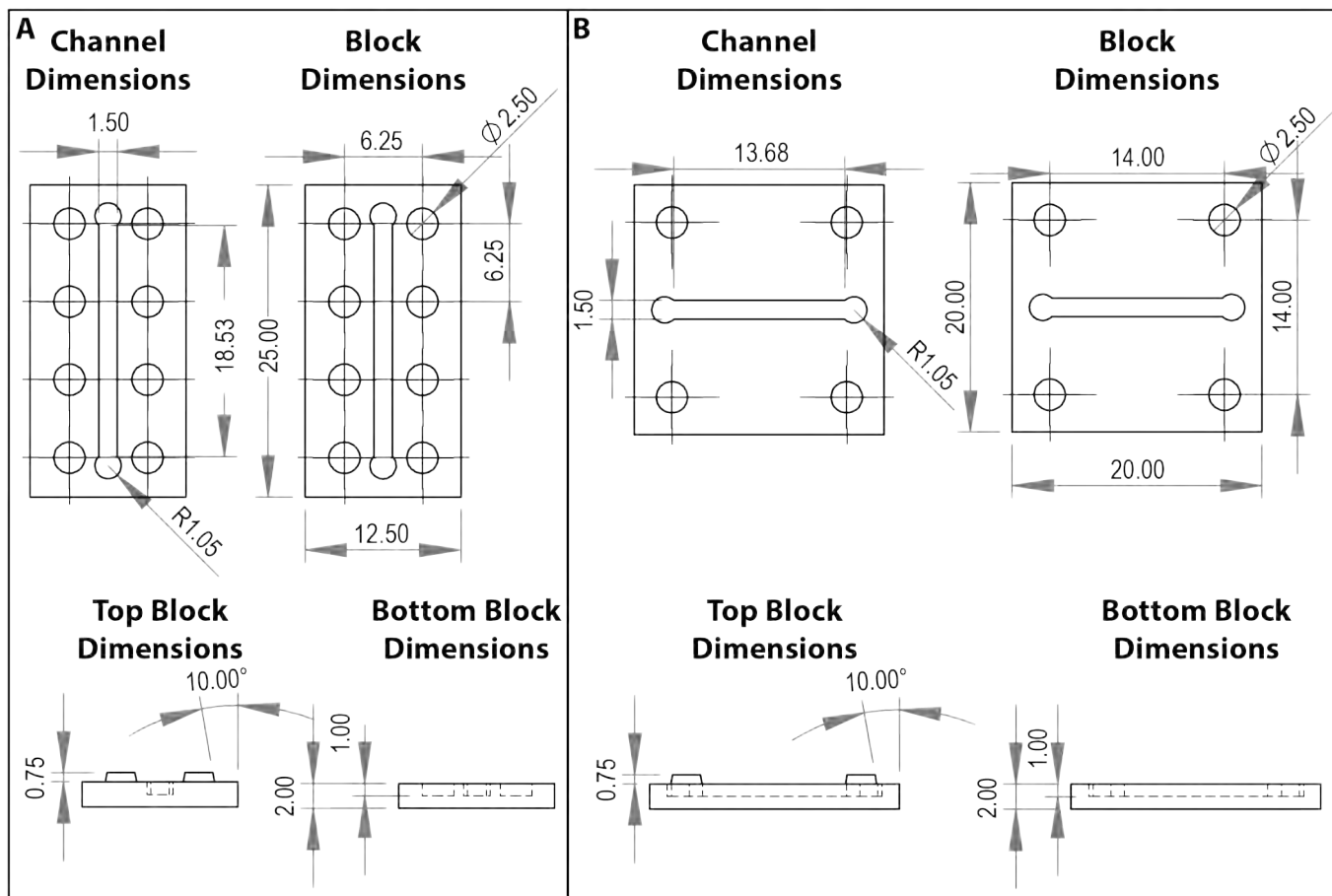


Fig. S18 Dimensioned drawings for Straight (A) and Stacked, Overlapping Straight (B) channel microfluidic devices. All units are in mm. Dashed lines indicate hidden lines.

1.18 Pattern Fidelity

To analyze the pattern fidelity of the PEGDA-PAA LEGO blocks, a straight-channel device was assembled and imaged from above or from the side. Length and width of the overall block were imaged from above and quantified using Image-J. All other dimensions were quantified using a contact angle goniometer to image from the side, and the dimensions were quantified using Image-J. Pattern fidelity was quantified by comparing the printed dimensions against those of initial CAD file. Note that D' and E' represent channel geometries after self-adhesion.

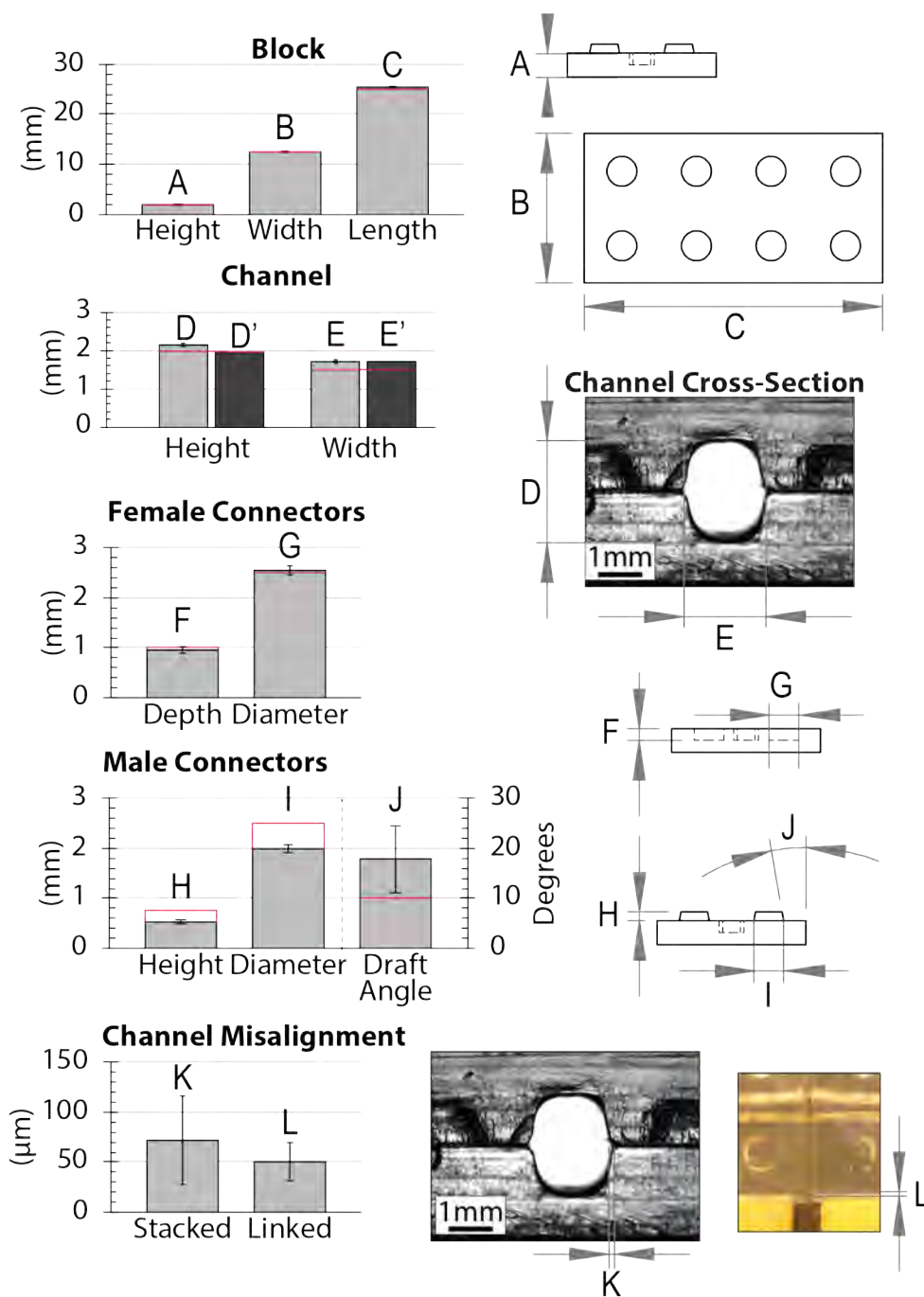


Fig. S19 Pattern fidelity analysis of a straight channel microfluidic device. Block, channel, and connector dimensions, as well as channel misalignment were measured using Image J. Error bars = standard deviation. Red line = original dimensions. Inset images are a side-view of a straight-channel device, and a top view of a stacked and linked device.

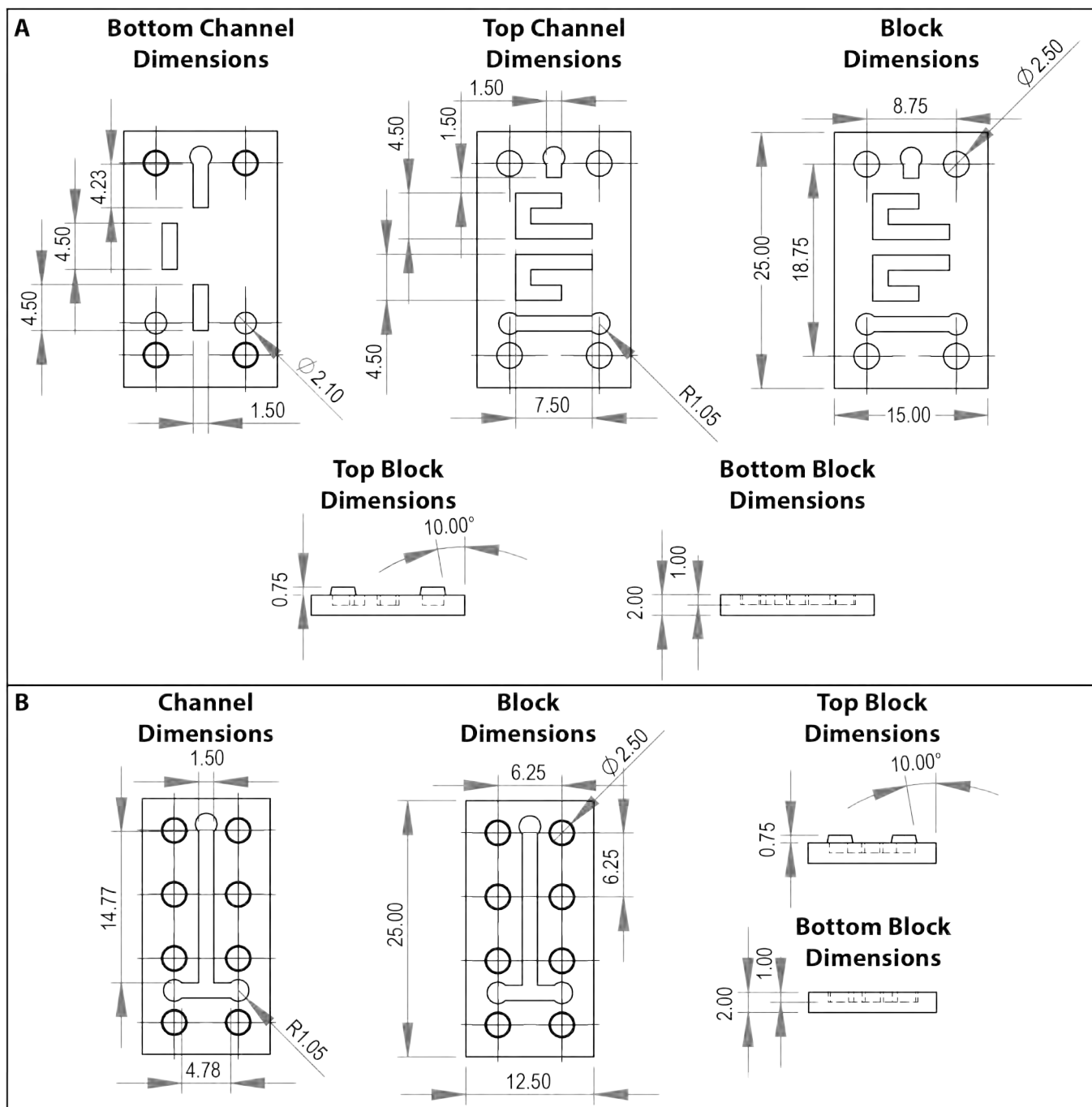


Fig. S21 Dimensioned drawings for Serpentine Mixer (A) and T-Junction (B) channel microfluidic devices. All units are in mm. Dashed lines indicate hidden lines.

1.19 COMSOL Modeling of Chaotic Advection

Three-dimensional microfluidic mixing simulations were conducted using the finite element analysis software (COMSOL Multiphysics, Burlington, MA). In particular, the “Laminar Flow” and “Transport of Diluted Species” modules were employed to solve for the steady state advection-diffusion equation

$$D_i \nabla^2 c_i = \mathbf{u} \cdot \nabla c_i, \quad (5)$$

where D_i , c_i and \mathbf{u} are the solute diffusivity, concentration and velocity vector field, respectively; along with the incompressible Navier Stokes equation

$$\rho \mathbf{u}(\nabla \cdot \mathbf{u}) = -\nabla p + \mu \nabla^2 \mathbf{u}, \quad (6)$$

where ρ , μ and p are the fluid density, dynamic viscosity and pressure, respectively. At the microfluidic channel walls, a no-flux boundary condition was imposed such that $\mathbf{n} \cdot (-D_i \nabla c_i + \mathbf{u} c_i) = 0$, where \mathbf{n} is the unit normal vector; in addition to a no-slip condition such that $\mathbf{u} = 0$. At the boundaries representing the device inlets, the solute concentration was constrained to $c_i = c_{i,0}$ and a laminar inflow condition was imposed, thus requiring the inlet velocity profile to be that of fully developed Poiseuille flow of average bulk velocity U . At the device outlet, diffusive transport is omitted such that $\mathbf{n} \cdot D_i \nabla c_i = 0$, and $p = 0$. After importing the 3D CAD model and setting the boundary conditions, a medium-resolution tetrahedral mesh was formed, ultimately generating approximately 10^5 degrees of freedom to be solved. Solutions for the concentration, velocity and pressure were obtained using an iterative, geometric multigrid solver.

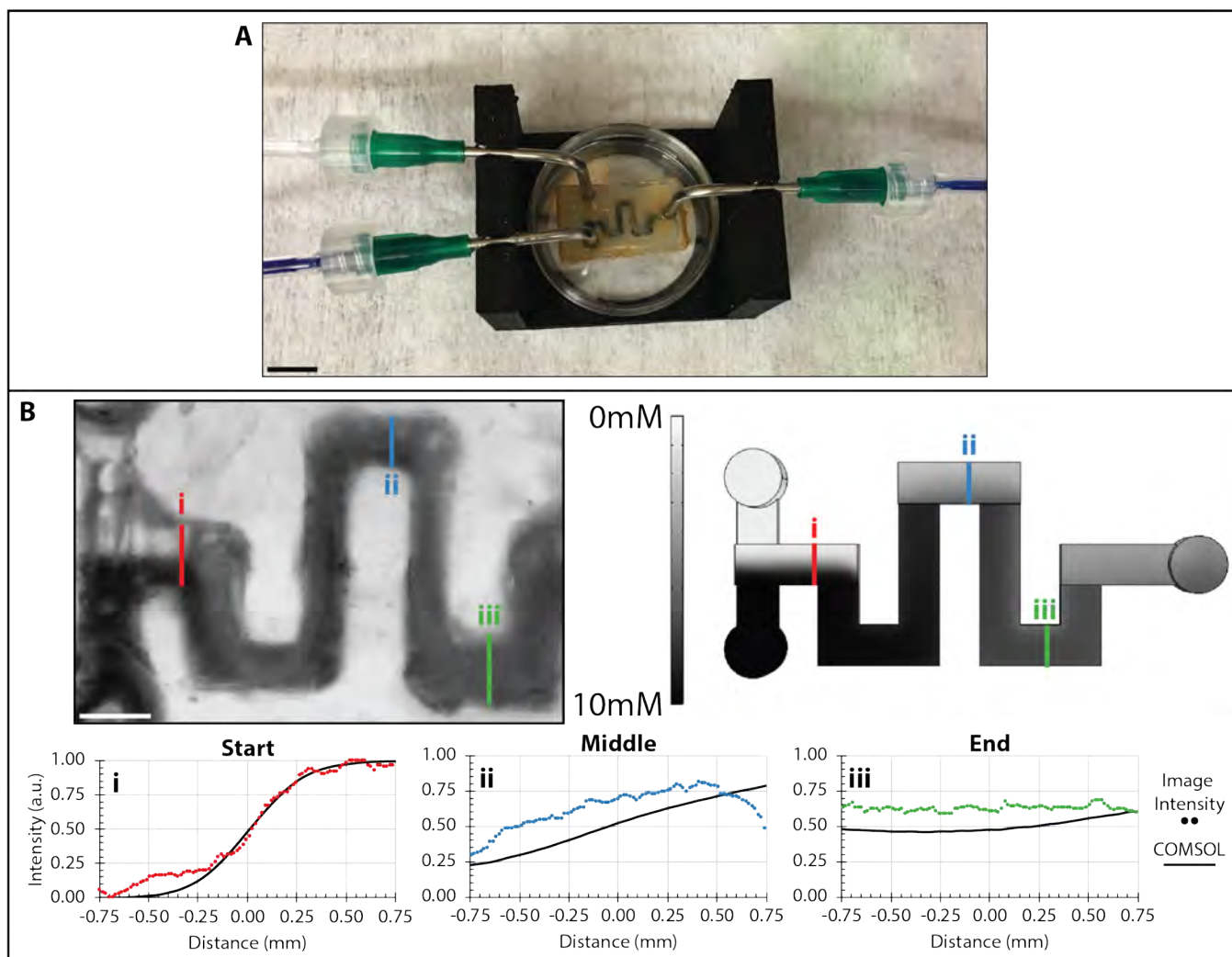


Fig. S22 (A) Serpentine mixer perfusion setup with 10mM Evans Blue and water at the inlets. Scale bar = 10mm. (B) Greyscale image of Evans Blue and water mixing through the serpentine mixer. Image intensity values were calculated at the (i) start, (ii) middle, and (iii) end of the mixer. The intensity data broadly matches up with a COMSOL model of evans blue diffusion in the serpentine mixer design. Scale bar = 2mm.

For both inlets the boundary conditions were set to Laminar inflow, the flow rates were set to $1.67 \times 10^{-9} \text{ m}^3/\text{s}$, with an entrance length of 0.005 m. The inflow concentration for Evans Blue was set to 10 mM with the isotropic diffusion coefficient of Evans Blue in water set to $1.64 \times 10^{-10} \text{ m}^2/\text{s}$ ^{15,16}. The inflow concentration for water was set to 0 mM.

The walls of the micromixer channel were set to No Flux since minimal diffusion of Evans Blue into these PEGDA-PAA hydrogels was observed experimentally. In addition, the high Peclet number for this serpentine mixer was further expected to minimize the relative contribution of diffusive flux of Evans Blue into the hydrogel. The Peclet and Reynolds numbers for the serpentine mixer are defined as:

$$Pe = \frac{Lu}{D} \approx 16,100 \quad Re = \frac{Lu\rho}{\mu} \approx 2.6 \quad (7)$$

Where L is the characteristic length, or hydraulic diameter of the channel ($\approx 0.0012 \text{ m}$), u is the average flow velocity in the mixing channel (0.0022 m/s), D is the isotropic diffusion coefficient of Evans Blue ($1.64 \times 10^{-10} \text{ m}^2/\text{sec}$)^{15,16}, ρ is the density of water (997 mg/m^3), and μ is the dynamic viscosity of water ($1 \times 10^{-3} \text{ Pa}\cdot\text{s}$). u was calculated based on the flow rate in the mixing channel (0.2 mL/min or $3.33 \times 10^{-9} \text{ m}^3/\text{s}$) and the cross-sectional area of the mixing channel (1.5 mm^2 or $1.5 \times 10^{-6} \text{ m}^2$, **Figure S21**). $Pe = 16,100$ suggests that the effect of diffusive transport is very small when considering the concentration of Evans Blue within the channels. At a flow rate of 0.2 mL/min the flow traveled from the inlet to the outlet in ≈ 30 seconds (total volume of the micromixer channel is $100 \mu\text{L}$), and over such short time scales the diffusion of Evans Blue through the walls of the hydrogel should be negligible.

The predicted Evans blue concentrations from the COMSOL simulation (smoothed using a 10-span moving average) were compared to the experimentally measured images using a Matlab script that extracted linescans of pixel intensity across the width of the channel at three locations (**Figure S22**). The raw data was normalized by subtracting the lowest intensity value from the water fraction of the flow at the start of the channel (**Figure S22B**), and then dividing by the maximum intensity value of the water fraction of the flow at the start of the channel.

Overall the COMSOL simulation is qualitatively consistent with the trends exhibited by the experimental measurements. At the start of the micromixer, the Evans Blue dye is sharply separated across the cross-section of the channel, with minimal (normalized) intensity of 0.0 at -0.75 mm and maximum (normalized) intensity of 1.0 at 0.75 mm . (**Figure S22Bi**). Roughly halfway through the micromixer, some mixing occurs and the minimal (normalized) intensity is ~ 0.25 at -0.75 mm and maximum (normalized) intensity of ~ 0.75 at 0.5 mm , which represents partial mixing and a more gradual spatial distribution (**Figure S22Bii**). It should be noted that the experimental data drops off at 0.75 mm , which may result from some aberrations in the channel geometry as 3D printed (**Figure S22Bii**). Finally, toward the end of the micromixer channel uniform mixing has been achieved with the Evans Blue intensity uniformly distributed across the channel, although the experimental values are slightly offset from the COMSOL data (**Figure S22Biii**).

1.20 T-Junction Microfluidic Device

A T-Junction LEGO-style microfluidic device was fabricated using the same strategy used for the other microfluidic blocks (**Figure S21B**, **S23**). Each inlet was perfused with 1 mM Evans Blue and 1 mM Eosin Y at 0.1 mL/min . Laminar flow was seen throughout the length of the device with very little mixing.

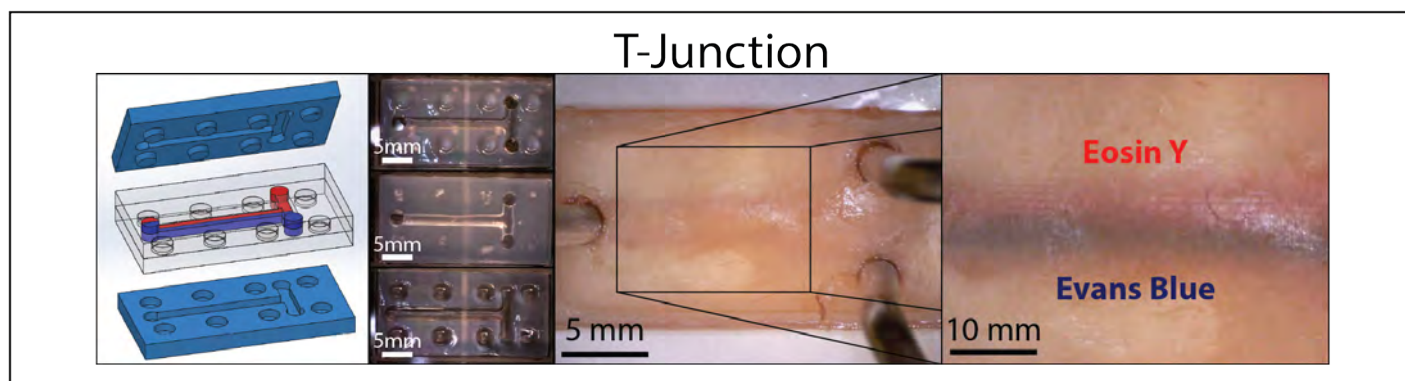


Fig. S23 A T-Junction microfluidic device were fabricated from two individual LEGO-style blocks. The inlets were perfused with 1 mM Evans Blue or Eosin Y at 0.1 mL/min . Laminar flow was maintained throughout the length of the device resulting in very little mixing of the flow.

References

- 1 T. Swift, L. Swanson, M. Geoghegan and S. Rimmer, *Soft Matter*, 2016, **12**, 2542–2549.
- 2 P. F. Jacobs, *Rapid prototyping & manufacturing: fundamentals of stereolithography*, Society of Manufacturing Engineers, 1992.
- 3 V. Chan, P. Zorlutuna, J. H. Jeong, H. Kong and R. Bashir, *Lab Chip*, 2010, **10**, 2062–2070.
- 4 G. Beamson, *The Scienta ESCA 300 Database*, 1992.
- 5 M. C. Biesinger, B. P. Payne, A. P. Grosvenor, L. W. Lau, A. R. Gerson and R. S. C. Smart, *Appl Surf Sci*, 2011, **257**, 2717–2730.
- 6 M. Omran, T. Fabritius, A. M. Elmahdy, N. A. Abdel-Khalek, M. El-Aref and A. E.-H. Elmanawi, *Appl Surf Sci*, 2015, **345**, 127–140.
- 7 A. Grosvenor, B. Kobe, M. Biesinger and N. McIntyre, *Surf Interface Anal*, 2004, **36**, 1564–1574.
- 8 T. Droubay and S. A. Chambers, *Phys Rev B*, 2001, **64**, 205414.
- 9 P.-H. Lo, W.-T. Tsai, J.-T. Lee and M.-P. Hung, *J Electrochem Soc*, 1995, **142**, 91–96.
- 10 G. K. Christiansen (Interlego AG), *Toy building brick*, US Patent 3,005,282; Assigned July 28, 1958.
- 11 Z. Wei, J. He, T. Liang, H. Oh, J. Athas, Z. Tong, C. Wang and Z. Nie, *Polym. Chem.*, 2013, **4**, 4601–5.
- 12 L. J. Kirwan, P. D. Fawell and W. van Bronswijk, *Langmuir*, 2003, **19**, 5802–5807.
- 13 Y. Wu, J. Liang, F. Horkay and M. Libera, *J Polym Sci B: Polym Phys*, 2016, **54**, 64–72.
- 14 ASTM, *ASTM D790-07*, 2007.
- 15 J. Levick and C. Michel, *Q J Exp Physiol CMS*, 1973, **58**, 67–85.
- 16 T. M. Valentin, S. E. Leggett, P.-Y. Chen, J. K. Sodhi, L. H. Stephens, H. D. McClintock, J. Y. Sim and I. Y. Wong, *Lab Chip*, 2017, **17**, 3474–3488.